



## The Effect of Plasma Boundaries on the Dynamic Evolution of Relativistic Radiation Belt Electrons

D. Wang\* (1), Y. Y. Shprits(1,2,3), I. S. Zhelavskaya(1,2), F. Effenberger(1), A. Castillo(1,2),  
A. Drozdov(3), N. Aseev(1,2), and S. Cervantes(1,2)

(1) GFZ German Research Centre for Geosciences, Potsdam, Germany; e-mail: dedong@gfz-potsdam.de

(2) University of Potsdam, Potsdam, Germany; e-mail: yshprits@gfz-potsdam.de

(3) University of California, Los Angeles, CA, USA

### Abstract

Understanding the dynamic evolution of relativistic electrons in the Earth's radiation belts during both storm and non-storm times is a challenging task. The U.S. National Science Foundation's Geospace Environment Modeling (GEM) focus group "Quantitative Assessment of Radiation Belt Modeling" (QARBM) has selected two storm time and two non-storm time events that occurred during the second year of the Van Allen Probes mission for in-depth study. Here, we perform simulations for these GEM challenge events using the 3-Dimensional Versatile Electron Radiation Belt (VERB-3D) code. We set up the outer  $L^*$  boundary using data from Geostationary Operational Environmental Satellites (GOES) and validate the simulation results against satellite observations from both the GOES and Van Allen Probe missions for 0.9 MeV electrons. Our results show that the position of the plasmopause plays a significant role in the dynamic evolution of relativistic electrons. The magnetopause shadowing effect is included by using last closed drift shells calculated from the TS07D model and it is shown to significantly contribute to the dropouts of relativistic electrons at high  $L^*$ .

### 1 Introduction

Understanding the dynamic evolution of relativistic electrons in the Earth's radiation belts under different geomagnetic conditions is challenging in magnetospheric physics, due to the delicate balance between various acceleration and loss processes. Different adiabatic and non-adiabatic processes have been proposed to cause the acceleration and loss of relativistic electrons [1,2,3].

"To concentrate community efforts and maximize scientific returns", the U.S. National Science Foundation's Geospace Environment Modeling (GEM) focus group "Quantitative Assessment of Radiation Belt Modeling" (QARBM) has selected two storm time and two non-storm time events that occurred during the second year of the Van Allen Probes mission for in-depth study [4]. A number of studies have been performed for these GEM challenge events [Tu et al 2019 and references therein].

In the present study, we extend previous works on these GEM challenge events by performing simulations using the VERB-3D code to investigate the effects of the plasmopause and magnetopause locations on the dynamic evolution of relativistic electrons in the outer radiation belt. In this study, instead of using event specific waves, we use empirical wave models. In addition, instead of using Van Allen Probe measurements to set up the upper  $L$  boundary, we use measurements from GOES satellites, which is the only one data-driven boundary in our simulations. This is meaningful in aspects of both science study and application. Extending outer boundary to a further region can lead to more understandings about the effect of the competing processes, especially between radial and local diffusion. It may be also helpful to infer the situation in radiation belts after radiation belt satellite mission are finished. In section 2, we describe the VERB-3D code and the parameters adopted for our numerical simulations. In section 3, we present simulation results and their validation against satellite observations. Results and other possible mechanisms are discussed in section 4. Finally, we summarize our findings and outline directions for future studies in section 5.

### 2 Model Description

The dynamic evolution of electrons in the radiation belts can be described by the bounce- and Magnetic Local Time (MLT)-averaged Fokker-Planck equation [5,6]:

$$\begin{aligned} \frac{\partial f}{\partial t} = & L^{*2} \frac{\partial}{\partial L^*} \Big|_{\mu, J} \left( D_{L^* L^*} L^{*-2} \frac{\partial f}{\partial L^*} \Big|_{\mu, J} \right) + \\ & \frac{1}{T(\alpha_0) \sin(2\alpha_0)} \frac{\partial}{\partial \alpha_0} \Big|_{p, L^*} T(\alpha_0) \sin(2\alpha_0) \left( D_{\alpha_0 \alpha_0} \frac{\partial f}{\partial \alpha_0} \Big|_{p, L^*} + \right. \\ & \left. D_{p \alpha_0} \frac{\partial f}{\partial p} \Big|_{\alpha_0, L^*} \right) + \frac{1}{p^2} \frac{\partial}{\partial p^2} \Big|_{\alpha_0, L^*} p^2 \left( D_{pp} \frac{\partial f}{\partial p} \Big|_{\alpha_0, L^*} + \right. \\ & \left. D_{p \alpha_0} \frac{\partial f}{\partial \alpha_0} \Big|_{p, L^*} \right) - \frac{f}{\tau}, \end{aligned} \quad (1)$$

Where  $f$  is the distribution function (phase space density),  $\mu$  and  $J$  are the first and second adiabatic invariants, and  $L^*$  is an invariant inversely proportional to the third adiabatic invariant,  $\Phi$ .  $D_{\alpha_0 \alpha_0}$  and  $D_{pp}$  are the bounce-

averaged pitch angle and momentum diffusion coefficients, respectively, and  $D_{p\alpha_0}$  is the mixed diffusion term. These aforementioned diffusion terms are local diffusion terms, while  $D_{L^*L^*}$  is the radial diffusion coefficient.  $T(\alpha_0)$  is a function related to the particle's bounce time,  $\tau$  is set as a quarter of the bounce period inside the loss cone and infinity outside the loss cone.

Several factors are taken into account in our simulations: (1) The plasmopause location separates chorus waves outside of the plasmasphere and hiss waves inside the plasmasphere. We use two different methods to obtain the plasmopause position for each timestep of the simulations. One method is to calculate the plasmopause position using the time series of the Kp index according to [Carpenter and Anderson, 1992]:

$$L_{pp} = 5.6 - 0.46Kp_{max}, \quad (2)$$

where  $L_{pp}$  is the location of the plasmopause and  $Kp_{max}$  is the maximum Kp value over the previous 24 hours. This empirical plasmopause model is limited to a minimum  $L_{pp} = 2$  at  $Kp_{max} \geq 7$ . During the event periods under study here, the maximum  $Kp_{max}$  value is 7. The other method to obtain the plasmopause position is using a recently developed Plasma density in the Inner magnetosphere Neural network-based Empirical (PINE) model adopting a Neural-network-based Upper-hybrid Resonance Determination (NURD) algorithm[8]. We calculated the MLT-averaged plasmopause position based on the NURD model[8]. We calculate the MLT-averaged plasmopause position using the output of the PINE model by applying the density threshold of  $40 \text{ cm}^{-3}$  to separate the plasmasphere from the outside of the plasmasphere.

(2) The last closed drift shell is calculated using the IRBEM library[9] and TS07D magnetic field model[10] and then used to simulate the effect of magnetopause shadowing. When  $L^*$  is larger than the last closed drift shell location, we set the PSD to zero before the step of radial diffusion in the simulation.

### 3 Comparison of Simulations with Observations

Figures 1-3 compare the simulated fluxes to the observed fluxes from both Van Allen Probes and GOES, for the considered GEM challenge events. In each figure, panel (a) shows the flux of electrons with energy at 0.9 MeV and an equatorial pitch-angle of 50 degree, as a function of  $L^*$  and time. Here,  $L^*$  is calculated using the TS07D magnetic field model [10]. Data from GOES and Van Allen Probes are consistent with each other at conjunction points. Panels (b) and (c) give the VERB-3D simulation results using plasmopause positions estimated following [Carpenter and Anderson, 1992] and calculated from the PINE plasmasphere model [8], respectively. Panels (d) and (e) show the normalized differences between observations and simulation results using different plasmopause positions. Blue color means that the simulation results underestimate the flux, while red and yellow colors

indicate that the simulation results overestimate the fluxes. In panels (b)-(e), the locations of the plasmopause are overplotted as black line. The positions of the last closed drift shell calculated using the TS07D magnetic field model are overplotted as magenta lines in panels (b)-(e). Panel (f) in each figure plots the variation of the Dst (red) and Kp (black) geomagnetic indices.

#### 3.1 Event 1 and 2: Nonstorm Time Enhancement and Dropout

Figure 1 shows the electron flux observations and VERB-3D simulation results for the period from September 7, 2013 to September 26, 2013, which includes two nonstorm GEM Challenge events: a nonstorm time enhancement event on September 20, 2013 and a nonstorm time dropout event on September 24, 2013.

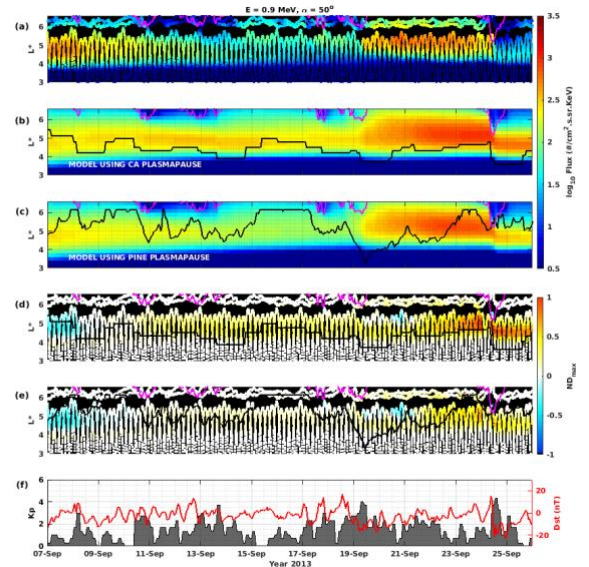


**Figure 1.** Particle observations and VERB simulations from September 7, 2013 to September 26, 2013 including both nonstorm GEM Challenge events (a nonstorm time enhancement event on September 20, 2013 and a nonstorm time dropout event on September 24, 2013). (a) Particle flux for 0.9 MeV, 50 degree pitch angle electrons from observations of Van Allen Probes, GOES 13 and 15. (b) VERB-3D simulation results using plasmopause positions calculated following Carpenter and Anderson [1992] for this period. (c) VERB-3D simulation results using the plasmopause position estimated from the new PINE plasmasphere model [5]. (d) Normalized difference between observations (shown in panel (a)) and simulations (shown in panel (b)). (e) Normalized difference between observations (shown in panel (a)) and simulations (shown in panel (c)). (f) Dst and Kp index during this period. The over-plotted magenta lines in panels (b)-(e) show the last closed drift shell. The over-

plotted black lines in panels (b)-(e) show the plasmopause positions.

Figure 1(a) illustrates that both GOES and Van Allen Probes observed a significant enhancement of relativistic electrons on September 19-20, 2013, which is followed by a dropout at higher  $L$ -shells ( $L^* > 5$ ) and a moderate decrease near  $L^*$  of 5 on 24 September 2013. Figure 1(b) shows simulation results using the plasmopause positions estimated following [Carpenter and Anderson, 1992]. It can be seen from figure 1(d) that during the first day under study, some underestimations occur in the heart of the belt (near  $L^*=5$ ), which shows that the assumed initial condition does not match very well with the observations. However, during the following day, the simulation results agree already well with the data. During the following eight days from September 11 to September 19, simulation results reproduced the dropouts at higher  $L$ -shells when  $L^* > LCDS^*$ . However, in the heart of the belt, overestimation occurs. This can be associated with the plasmopause positions. Outside the plasmopause, chorus wave acceleration leads to overestimation. Thus, the enhancement in the heart of the belt on September 20, 2013 is not very pronounced in this simulation. It can be seen from figure 1(c) and (e) that using the new plasmopause position improved the agreement between observations and simulations significantly, especially before the enhancement event. There is still some overestimation, which may result from the diffusion coefficients of hiss waves. For the dropout event during 24 September, the dropout at higher  $L$ -shells is reproduced in both simulations by involving the magnetopause shadowing effect. However, a decrease of flux at  $L$ -shell range [4, 5] is not well reproduced. This will be discussed in section 4.

### 3.2 Storm Time Dropout

On 1 June 2013, a strong geomagnetic storm happened with a minimum Dst index of -110 nT and a maximum Kp index of 7. An electron flux dropout occurred on 1 June 2013, as shown in figure 2(a).

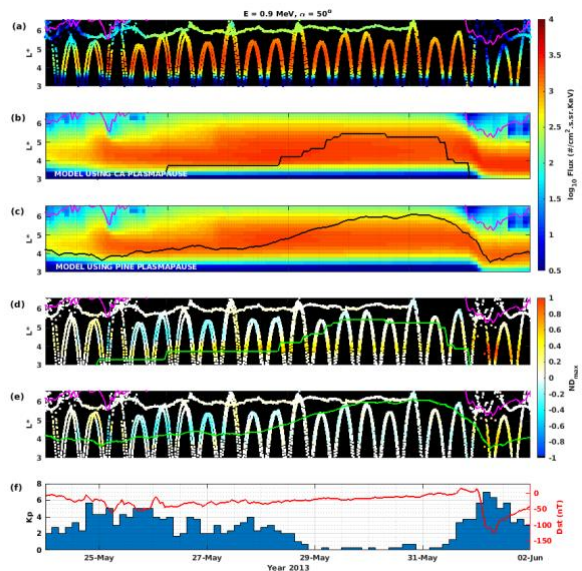


**Figure 2.** Same format as figure 1 but for the storm time dropout GEM challenge event (on June 1, 2013) from May 25, 2013 to June 2, 2013.

During this period, GOES 13 data is not available. Panels (b) and (c) show results of VERB-3D simulations using different plasmopause positions (overplotted as black lines). The overplotted magenta lines give the LCDS locations calculated in TS07D magnetic field model. It can be seen that using the positions of the LCDS, the simulation can reproduce the dropouts outside the LCDS well. However, the simulation results did not reproduce the dropout where  $L^* < LCDS$  during the storm main phase and exhibit overestimation during the recovery phase. This overestimation may be attributed to errors in the magnetic field model, other loss mechanisms such as wave-particle interaction in plasmaspheric plumes, or underestimated outward radial diffusion rates during these periods. The simulation results using the plasmopause position following [Carpenter and Anderson, 1992] have some overestimations before the storm near  $L^* = 4$ . When using the plasmopause estimated from the new NURD plasmasphere model, the agreement between simulation results and observations is improved.

### 3.3 Storm Time Enhancement

On 17 Mar 2013, a strong storm occurred with a minimum Dst index of -130 nT and a maximum Kp index of 7-. During this day, after a sharp dropout, the flux of relativistic electrons recovered and enhanced significantly by 2 orders of magnitude. Figure 3(a) shows GOES and Van Allen Probes measurements of electrons with energy at 0.9 MeV and pitch-angle at 50 degree.

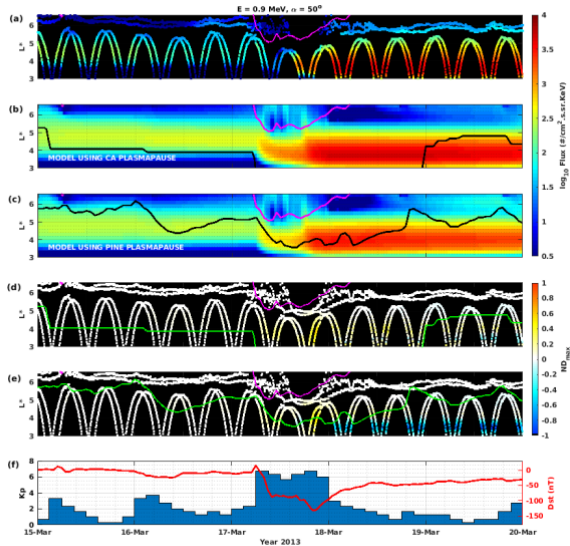


**Figure 3.** Same format as figure 1 but for the storm time dropout GEM challenge event (on June 1, 2013) from May 25, 2013 to June 2, 2013.

Before 12:00 UT on 17 March, the fluxes of relativistic electrons were dramatically depleted, especially at high  $L$ -shells ( $L^* > 5$ ). This depletion is suggested to result from the magnetopause shadowing effect. However, previous simulation studies for this event did not investigate the effect of magnetopause shadowing. In our simulations, we include the effect of magnetopause shadowing to investigate the reason for the sharp dropout before the enhancement event and test the influence of the different plasmopause positions. Figures 2(b) and 2(c) show the results of VERB-3D simulations using different plasmopause positions. As seen readily in these figures, the depletion of electron fluxes can be well reproduced by the loss to the last closed drift shell (indicated as overplotted magenta lines). After this depletion, the flux of relativistic electrons enhanced by nearly 2 orders of magnitude during the 12 hours interval on Mar 17 in the  $L$ -shell range [3, 5]. The peak location of the outer radiation belt moves Earthward compared with the location before this storm. The simulation results indicate that the enhancement of relativistic electrons is well reproduced.

## 4 Discussion

During several hours on 24 September 2013, the radiation belt electrons with energy from 500 keV to several MeV exhibited a significant dropout at higher  $L$ -shells ( $L^* > 5$ ) and a moderate decrease near  $L^*$  of 5. Our simulations incorporating magnetopause shadowing effect by using the last closed drift shell reproduced the dropout at higher  $L$ -shells. However, a decrease of flux at  $L$ -shell range [4, 5] is not well reproduced. This may result from underestimation of outward radial diffusion, or lack of wave-particle interactions in plasmaspheric plumes. On

the other hand, EMIC waves are observed during the interval of this dropout. The effect of EMIC waves in this dropout event are still under debate. Dips in the Phase Space Density (PSD) profile were found for electrons with energy higher than 2 MeV but no dips in PSD were found for electrons with energies near 1 MeV. The investigation of the electron depletion at low  $L$ -shell during this event will be a subject of the further research.

During storm times, the plasmasphere becomes more asymmetric due to the enhanced convection. During storm times, the plasmasphere is strongly eroded at all MLTs except for the dusk sector, where a bulge or plume is formed and extends further to the noon sector. Plasmaspheric bulge or plumes may form and extend to higher  $L$ -shells during storm time. However, in our 3D simulations using the PINE output, the plasmopause positions are averaged over MLT. This may lead to some overestimations of plasmopause positions during storm times, which can lead to an underestimation of the accelerations by chorus waves. In addition, our simulations in this study did not account for hiss waves in the plasmaspheric plume, which may cause some underestimations of losses.

## 5 Summary and Conclusion

The results of our study show that:

- The magnetopause shadowing effect plays an important role for dropout at higher  $L$ -shells. The last closed drift shell calculated using the TS07D magnetic field model can be used to simulate the magnetopause shadowing effect.
- The positions of the plasmopause plays an important role in the dynamic evolution of radiation belt electrons, especially during geomagnetically quiet times.
- Flux measurements from GOES observations can be used to set up outer boundary conditions for the simulation of radiation belts. During times when the Van Allen Probes data is not available, we can still use measurements from GOES to set up outer boundaries and infer the radiation belt dynamics at lower  $L$ -shells.

In future studies, we will test the usage of the innermost position of the plasmopause and include plumes by changing the MLT percentage of chorus waves and hiss waves in different time steps of simulations. Additionally, 4D simulations including the MLT dependence will be performed to check the effect of the MLT-dependent plasmopause positions and plasmaspheric plumes on the dynamic evolution of the radiation belts in detail.

## 6 Acknowledgements

We acknowledge the Geospace Environment Modeling Focus Group on the "Quantitative Assessment of Radiation Belt Modeling" for motivating this study. We

sincerely acknowledge Adam Kellerman for the preparation of the used satellite data and the calculation of last closed drift shells. We would like to thank Hayley Allison for the useful discussions. This project has received funding from the European Union's Horizon 2020 research and innovation programme under grant agreement No. 637302, NASA H-SR funding NNX15AI94G, and the Helmholtz-Gemeinschaft (HGF) [10.13039/501100001656]. All Van Allen Probes data were accessed through the MagEIS website (<https://rbspsect.lanl.gov>), and we graciously thank the MagEIS instrument team. The Kp index was provided by GFZ Section 2.3 and downloaded from the World Data Center (<http://wdc.kugi.kyoto-u.ac.jp/>). NURD plasma density data can be downloaded from <ftp://ftp.gfz-potsdam.de/home/rbm/NURD/>.

## 7 References

1. Y. Y. Shprits, S. R. Elkington, N. P. Meredith, and D. A. Subbotin, "Review of modeling of losses and sources of relativistic electrons in the outer radiation belts: I. Radial transport," *J. Atmos. Sol. Terr. Phys.*, **70**, 14, 2008, pp. 1679-1693, doi:10.1016/j.jastp.2008.06.008.
2. Y. Y. Shprits, D. A. Subbotin, N. P. Meredith, and S. R. Elkington, "Review of modeling of losses and sources of relativistic electrons in the outer radiation belts: II: Local acceleration and loss," *J. Atmos. Sol. Terr. Phys.*, **70**, 14, 2008, pp. 1694-1713, doi:10.1016/j.jastp.2008.06.014.
3. R. M. Thorne, "Radiation belt dynamics: The importance of wave-particle interactions," *Geophys. Res. Lett.*, **37**, 2010, L22107, doi:10.1029/2010GL044990.
4. W. Tu, W. Li, J. M. Albert, and S. Morley, "Quantitative assessment of radiation belt modeling," *Journal of Geophysical Research: Space Physics*, **124**, 2019, pp. 898–904, doi:10.1029/2018JA026414.
5. M. Schulz, and L. J. Lanzerotti, "Particle diffusion in the radiation belts," *Physics and Chemistry in Space* (Vol. 7). 1974. Berlin, Heidelberg: Springer Berlin Heidelberg.
6. Y. Y. Shprits, D. Subbotin, and B. Ni, "Evolution of electron fluxes in the outer radiation belt computed with the VERB code," *J. Geophys. Res.*, **114**, 2009, A11209, doi:10.1029/2008JA013784.
7. D. L. Carpenter, and R. R. Anderson, "An ISEE/whistler model of equatorial electron density in the magnetosphere," *J. Geophys. Res.*, **97**(A2), 1992, pp. 1097-1108, doi:10.1029/91JA01548.
8. I. S. Zhelavskaya, Y. Y. Shprits, and M. Spasojevic, "Empirical modeling of the plasmasphere dynamics using neural networks," *Journal of Geophysical Research: Space Physics*, **122**, 2017, pp. 11,227–11,244, doi:10.1002/2017JA024406.
9. D. Boscher, S. Bourdarie, P. O'Brien, and T. Guild, "TRBEM Library v4.3", 2004-2008, ONERA-DESP, Toulouse France, Aerospace Corporation, Washington, DC.
10. N. Tsyganenko, and M. Sitnov, "Magnetospheric configurations from a high-resolution data-based magnetic field model," *Journal of Geophysical Research: Space Physics*, **122**(A6), 2007, A06225, doi:10.1029/2007JA012260.